Accepted Manuscript

Investigation of the dynamic mechanical properties of epoxy resins modified with elastomers

G. Mansour, K. Tsongas, D. Tzetzis

PII: S1359-8368(16)30048-8

DOI: 10.1016/j.compositesb.2016.03.024

Reference: JCOMB 4125

To appear in: *Composites Part B*

Received Date: 5 December 2015

Revised Date: 26 February 2016

Accepted Date: 11 March 2016

Please cite this article as: Mansour G, Tsongas K, Tzetzis D, Investigation of the dynamic mechanical properties of epoxy resins modified with elastomers, *Composites Part B* (2016), doi: 10.1016/j.compositesb.2016.03.024.

Keywords: A. Epoxy resin; A. Rubber toughening; B. Vibration; C. Genetic algorithm; D. Non-destructive testing.

ABSTRACT

The mechanical and modal properties of epoxy resin reinforced with different content of carboxyl-terminated butadiene acrylonitrile copolymer (CTBN) rubber were investigated in this paper with an analytical-experimental identification method. Mechanical tensile tests were conducted for concentrations between 0 and 25wt% of CTBN rubber. The dynamic responses of the epoxy/CTBN rubber composites were measured by vibrating cantilever beam specimens with an impact force through a modal hammer, while the vibratory response was detected through an acceleration transducer. The analytical-experimental transfer function method is utilized for the deduction and therefore comparison of the elasticity modulus of the epoxy/rubber composites. The procedure for the identification of analytical-experimental transfer functions was carried out using a genetic algorithm (GA) by minimizing the difference between the measured response from tests and the calculated response, which is a function of the modal parameters. Both tensile and modal tests have shown, while it was evident from the results that the CTBN composites could absorb greater amounts of strain energy. The modal test results indicate that CTBN rubber particles can improve the damping capacity of the epoxy-based composites. However, it was observed that the stiffness of the epoxy/CTBN rubber composites was dramatically reduced.

INVESTIGATION OF THE DYNAMIC MECHANICAL PROPERTIES OF EPOXY RESINS MODIFIED WITH ELASTOMERS

G. Mansour[a], K. Tsongas[a], D. Tzetzis[b1]

[a]Laboratory for Machine Tools and Manufacturing Engineering, Department of Mechanical Engineering, Aristotle University of Thessaloniki, University Campus, 54124, Thessaloniki, Greece.

[b]International Hellenic University, 14km Thessaloniki - N.Moudania, 57001, Thermi, Greece.

1. INTRODUCTION

In response to a transient or dynamic loading, there is a wide set of structural components or assemblies for which vibration is directly related to performance, either by virtue of causing temporary malfunction during excessive motion or by creating disturbance or discomfort, such as stress fatigue failure, premature wear, operator discomfort, unsafe operating condition, high noise levels. For all these potential problems, it is important the vibration levels encountered in service or operation to be anticipated and brought under satisfactory control [1]. Thus, it is important to determine three modal parameters; resonance frequencies of the structure to avoid resonance, damping factors and mode shapes to reinforce the most flexible points or to determine the suitable points to reduce weight or to increase damping. With respect to these dynamic aspects, composite materials represent an excellent possibility designing components requiring for dynamic behavior.

In the past, the damping capacity of conventional engineering materials has not generally provided sufficient energy dissipation to limit resonant or near-resonant amplitudes of vibration [2]. It would therefore be of interest to investigate new materials simultaneously exhibiting high damping capacity with high stiffness and low density which includes polymer matrix nanocomposites. High damping capacity is an important factor for various industrial applications; therefore, it is necessary to develop structural components with a high level of mechanical damping. High loss factor polymers have been used in the past for modern damping applications [3-7]. Nowadays there are plenty of other advanced materials that could be utilised for damping applications. Researchers have, therefore, concentrated their efforts towards the development of polymers in which nanomaterials are embedded in polymer substrates and promising results have been established primarily improving the mechanical properties [8-11]. However, for

[1] Corresponding author at: International Hellenic University, 57001, Thessaloniki, Greece.
Telephone number: +30 2310807548
Email address: d.tzetzis@ihu.edu.gr

increasing damping, epoxy resins reinforced with CTBN rubber are promising materials due to their large recoverable strain and high damping response. Adding rubber particulates (reactive liquid rubber CTBN) into polymer resin is an approach to effectively improve the damping behavior of composites [12]. In general, embedding such CTBN inclusions into a polymeric matrix system, can effectively improve the ductility as well as the fracture toughness of the polymeric composites [13-14]. The fracture toughness is an important property in fibre polymer composite industry, since it prevents delamination damage, while it is also vital in composite repair procedures [15-18].

The current work aims to investigate the dynamic and mechanical behavior of epoxy resins reinforced with CTBN rubber particles through an optimization algorithm for modal analysis and identification of experimentally defined transfer functions. The proposed modal analysis algorithm derives modal parameters from the transfer functions (TFs) of the composites by a curve-fitting technique. According to the authors' knowledge the influence of the CTBN rubber on the damping response of epoxy based composites is rarely discussed in the literature. Samples of 10 - 25wt% CTBN have been used to reinforce a DGEBA/F epoxy resin. The dynamic mechanical properties of the rubber modified epoxies were determined by both tensile and vibration tests. An analytical-experimental transfer function method is utilized for the deduction and therefore comparison of the elasticity modulus of the epoxy/rubber composites.

2. MATERIALS AND TEST METHODS

2.1. Preparation of the rubber-modified epoxy composites

The epoxy resin that has been used to form the rubber reinforced composites was a standard diglycidyl ether of bisphenol A/F (DGEBA/F) with an epoxide equivalent weight (EEW) of 169,7 g/eq., supplied by Gurit, UK. The reactive liquid rubber, which generates the micrometer-sized spherical rubber particles upon curing of the formulation, was a carboxyl-terminated butadiene-acrylonitrile (CTBN) rubber. It was supplied as 40wt% CTBN-epoxy adduct, 'Albipox 1000' (EEW =330 g/eq), from Evonik, Germany. The curing agent was a 3-aminomethyl-3,5,5-trimethylcyclohexylamine (SP115 hardener with an amine-hydrogen equivalent weight of 42,3 g/eq.), also supplied by Gurit, UK. In order to prepare a series of composites with 10 – 25wt% rubber content, the SP115 epoxy resin was mechanically mixed with Albipox 1000 - DGEBA/F masterbatch for 30min. The mixture was degassed for 15 min in a vacuum oven and then was blended in a stoichiometric amount of SP115 hardener (based on the amount

of DGEBA and the masterbatch) for 10 min. The rubber-modified resin was afterwards degassed in the vacuum oven before curing to remove any air entrapped in the mixture and then poured into a silicon mould. Finally, the resin system was cured at room temperature for 24hours following 16 hours at 50ºC with a ramp rate of 1ºC/min followed by a cooling step to room temperature to room temperature at 1ºC/min. Subsequently, rectangular specimens with the dimension of 160 x 20 x 4 mm^3 were utilized for the vibration tests were fabricated. For each particulate epoxy/rubber composite at least three specimens were prepared.

2.2. Tensile Tests

Tensile tests were performed at room temperature (23°C) on a Zwick Z010 (Zwick, Germany) universal testing machine at a constant crosshead speed of 1 mm/min. The measurements followed the ISO 527 testing standard using dumbbell shaped specimens. The specimens with 4 mm thickness were fabricated using a silicone mold. The overall length of dumbbell specimens was 150 mm. The length and width of the narrowed section were 10 and 4 mm, respectively. E-moduli were calculated within the linear section of the tensile stress-strain curves. All presented data corresponds to the average of at least five measurements.

2.3. Fractographic analysis

The local microstructure of the specimens was qualitatively examined using a JEOL JSM-840A scanning electron microscope (SEM). Prior to the test, the fractured surfaces of the samples were gold coated in an ion sputtering unit for over 6 min. The fractured surfaces were observed at suitable magnifications. The fractographs revealing the respective characteristic details of each sample were taken after suitable adjustments in probe current, voltage, image contrast and brightness as well as working distance. In this manner, images were taken on tension-failed, unmodified and rubber modified epoxy samples.

2.4. Modal tests and signal processing

The experimental apparatus for the forced vibration tests is shown in Fig.1, where the specimen is clamped on rigid support as a cantilever beam and vibrated by the impact hammer with a high-quality piezoelectric force transducer (Endevco Model 2302-10). The force-hammer was used to apply an initial vibration (input signal) on the free boundary where the specimen was subjected to free damped vibration. In addition, the vibratory response at the specimen tip (output signal) was detected through an

acceleration transducer with a sensitivity of 100 mV/g (Brüel & Kjaer 4507B), mounted on the free boundary, while the sensing cables were kept in a free state, thereby having a little influence on the vibration test. For impact excitation, an acquisition and realtime-analysis routine provided digital filtering for two-channel acquisition.

So both the force and acceleration analog signals are acquired by an analog-to-digital converter (FFT analyzer PULSE Brüel & Kjaer), while the corresponding results were recorded in a computer. The frequency range of acceleration signals was up to 3200 Hz, the sampling time interval was 0.12207 μs and the sampling frequency was 8192 samples per second (Hz). The modal hammer was calibrated by adjusting the level of the signal trigger force. Each specimen was tested 10 times and linear averaging was performed.

In order to obtain the specimen's modal properties from the transient vibration, the Fourier Transforms of both the excitation and the response signals were calculated. The ratio of response to excitation functions is computed to obtain an expression from the corresponding transfer function. The response can be calculated in terms of displacement, velocity or acceleration and as a result different terms have been used for the ratios of response to force. This study is focused on displacement responses and any reference to the TF expresses the receptance (dynamic compliance) of the system. The displacement is determined through a double integration process of the experimental data of the accelerometer sensor. High pass filters have been used to remove the direct current (DC) components and avoid the integrated errors. Thus, the ratio of the resulted displacement to the applied force is computed in order to obtain the receptance transfer function.

3. PROPOSED METHOD AND VERIFICATION OF IDENTIFICATION RESULTS

3.1. Experimental transfer functions

A transfer function G for a single degree of freedom system can be plotted in the Argand (complex) plane by its real and imaginary components as shown in Fig.2. The Argand or Nyquist plane plot is a very effective way of displaying the important resonance region. The amplitude is plotted as the vector X_i at angle θ_i from the real axis, where θ_i is the phase angle between exciting force and the displacement response at frequency ω_i. Through a circle-fitting method a modal circle can be established, which provides the means of extracting the required modal parameters of the system. This method

exploits the fact that in the vicinity of a resonance the behavior of most systems is dominated by a single mode. The response of each mode as it passes through resonance will lie on an arc of a circle [19].

The first step of the algorithm is the automatic selection of a fixed number of points on either side of any identified maximum arc length on the curve for equal frequency increments. Thus, the points ω_{d-1} and ω_{d+1} correspond to the largest arc length l_{imax}, while the resonance frequency ω_d would be in-between ω_{d-1} and ω_{d+1}.

At the second step the procedure followed was to fit a circle through the selected points of the resonance region of the curve and establish the center and the radius of the circle, considered as a least square minimization problem. By calculating the radii through the points on the arc, l_{imax}, the largest angle a included between two adjacent radii can be defined. The loss factor (n) can be computed from:

$$n = \frac{2\Delta\omega}{\omega_d \tan(a/2)} = \frac{2(\omega_{d+1} - \omega_{d-1})}{\omega_d \tan(a/2)} \quad (\text{for } a/2 < 45°) \tag{1}$$

An equivalent Young's modulus is identified from measured complex transfer functions. The constant quantity $G(\omega_i)$ at $\omega_i = 0$ defines the static response factor $G(0)$, which corresponds to distance OP in Fig.2. This real particular parameter is considered as the proportional gain of the system and it is identical with the compliance 1/K, the inverse value of the spring K of the vibratory system for a single degree of freedom. For fixed-free boundary conditions, stiffness of the system is $K = 3EI/L^3$, where $I = bh^3/12$ is the moment of inertia for a rectangular beam and L is the free length of the cantilever beam. Thus, the elastic modulus can be determined from the first mode of the transfer function by the following equation:

$$E = KL^3/3I \tag{2}$$

The viscoelastic response of materials under test can be expressed by the following equation:

$$n = \frac{E''}{E'} \tag{3}$$

where the quantity E' is called storage modulus, because it defines the energy stored in the specimen due to the applied strain and it is conceptually identical to E elastic modulus. The quantity E'' defines the dissipation of energy and is called the loss modulus.

3.2. Validation of the proposed method

For analytical mode characterization, a genetic algorithm (GA) optimization technique has been used to fit experimental transfer function data with a set of superimposed, single-mode response

functions. It can be shown [20] that the analytical receptance function of n-DOF system for input $f_i(t)$ and output $x_j(t)$ can be written as

$$G_{ij}(j\omega) = \frac{X_j}{F_i}(j\omega) = \sum_{k=1}^{N}\left(\frac{U_{ijk}+jV_{ijk}}{\delta_k + j(\omega-\omega_{dk})} + \frac{U_{ijk}-jV_{ijk}}{(\delta_k + j(\omega+\omega_{dk})}\right) \quad (4)$$

where U_{ijk}, V_{ijk} are the amplitudes of the residue of the k-th mode, δ_k is the attenuation exponent of the k-th mode, ω is the angular frequency, ω_{dk} is the damped natural frequency of the k-th mode, and N is the order of the curve fit. For an underdamped (light damping) mode k, the attenuation exponent and the damped natural frequency can be related with the loss factor n_k by $\delta_k = (n_k/2)\omega_{nk}$ and $\omega_{dk} = \omega_{nk}\sqrt{(1-(n_k/2)^2}$. The individual terms of the receptance matrix, i.e. the receptance functions, are the dynamic equivalent of the static flexibility influence coefficients [21]. Each column of the receptance matrix represents the ratio of the complex displacement response to force at the point j on the specimen at a single frequency, when the structure is excited at any point i. Thus, the elements of the principal diagonal (when i=j) represent the point receptances, while the off-diagonal elements represent the transfer receptances. The task undertaken is basically to find the optimal variables U, V in this theoretical expression of the transfer function, which matches closely the measured data. It is common in many minimization problems that the least-square error between two responses is selected as a measure of the response difference. Therefore, the summation of the square of the difference between the calculated and measured receptances over a concerned frequency range can be defined as an identification index. The objective function selected in this study can be described by:

$$Objective\ function\ f = \sum_{k=1}^{N}\left(1 - \frac{G_{ij}(j\omega)_{experimental}}{G_{ij}(j\omega)_{analytical}}\right)^2 \quad (5)$$

where $G_{ij}(j\omega)$ are the experimental and analytical transfer functions. GA has the advantage of seeking the whole space of solutions as well as not being entrapped in a local minimum. The flowchart of the whole identification process of the GA is illustrated in Fig.3. The input data for the algorithm are the attenuation exponent, the resonance frequency of k-th mode, the measured data, the number of independent variables and GA optimization parameters, such as the population size, the crossover rate, the mutation, etc. and the number of the GA loops are included. Using Eq.4 the fitness function is defined as shown in Eq.5 and is used in all steps of the algorithm. In the first loop of the GA, starting populations are randomly generated to set variables values, which are used to calculate the fitness function value. GA

uses selection, elitism, crossover and mutation procedures to create new generations. The new generations converge towards a minimum that is not necessarily the global one. After repetitions when the maximum generations' number is achieved the variables' values corresponding to the minimum fitness function value (ε) are selected as the optimum variables values of the GA. The usage of random numbers in GAs to produce the individuals of each generation gives the ability to explore the whole space of solutions [22].

The validation of the proposed method is verified by the calculation of the modal properties of a 10 degrees of freedom (DOF) mass-spring-dashpot model. The model's dynamic properties (inertia, stiffness, and damping) are shown in Table 1.

The equations of motion of an un-forced N degree of freedom elastic structure with viscous damping are

$$M\ddot{x}(t) + C\dot{x}(t) + Kx(t) = 0 \tag{6}$$

with initial conditions $x(0) = d_0$ and $\dot{x}(0) = v_0$. If the structure is modelled with N degrees of freedom, then there will be N natural frequencies and N modal vectors. The modal matrix $\bar{\Phi}$ is the column-wise concatenation of the N mode-shape vectors, $\bar{\Phi} = [\bar{x}_1\ \bar{x}_2 \cdots \bar{x}_N]$. The modal matrix $\bar{\Phi}$ diagonalizes both the mass and stiffness matrices. When the damping matrix is not proportional to the mass or the stiffness matrix, $\bar{\Phi}^T C \bar{\Phi}$ is not a diagonal matrix, the natural frequencies, loss factors, and modal vectors depend on the mass, damping and stiffness matrices of the structural system. For this 10-DOF system, the coupled equations of motion (Eq.6) were solved using the state-space method to uncouple them. Basically, the concept was to convert the set of N second order differential equations to an equivalent set on $2N$ first order differential equations, by assigning new variables (referred to as state variables) to each of the original variables and their derivatives. Subsequently, these numerically defined TFs were imported into the proposed algorithm as input measured data, so new modal parameters and TFs were identified. The results of the identification procedure are illustrated in Fig.4. The GA returned an optimal analytical transfer function which accurately fitted the numerical data of the mode superposition technique. The table in Fig.4 shows the transfer function parameters, as damped natural frequencies and the damping factors. From the values in the table, a conclusion can be drawn by comparing the current identification results with those calculated numerically; it is clear that they are very close to each other.

However, it was observed that the 10th modal circle has not been identified by the GA. This can be attributed to the range of discretization around the resonance region. This range should not be excessively limited since it becomes highly sensitive to the accuracy of the few points used, especially for low-amplitude modal circles, such as the modes 8-10. No less than 20 points should be used if needed to identify minor modal circles. The increase of the range of discretization points led to the identification of the 10th mode, while the accuracy of the identified modes 8 and 9 was significantly improved.

4. RESULTS AND DISCUSSION

4.1. Material mechanical behavior of the epoxy/rubber composites

The stress–strain behavior of all epoxy/rubber composites under uniaxial tension is shown in Fig.5. The specimens with high CTBN concentrations revealed a characteristic plastic behavior. The addition of the CTBN decreases the strength as reported in other studies [23]. The strength decreases with noticeable improvement in the strain to failure, revealing a characteristic toughening effect. The synergic effects of localized cavitations at the rubber/matrix interface and plastic shear yielding in the epoxy matrix are supposed to be responsible for a deformation that results in energy dissipation process which ultimately improves the toughness values of the rubber-modified epoxies. Additionally, the strength decrease can partly be explained by the fact that with increasing CTBN content, there is less available epoxy resin to sustain the uniaxial forces. Subsequently, the reduction in the strength values of CTBN-modified epoxies may be attributed to the lowering in cross-linking density of the epoxy network and justifies the high strains to failure attained.

Furthermore, it is clear that the neat resin system exhibits a brittle tensile behavior characterized by a Young's modulus value of 3815 MPa as compared to the rubber composites. The addition of CTBN decreases the Young's modulus indicating a ductile nature of the modified systems. Generally, when a rubber modifier is added to a thermoset resin, its elastomeric character authorizes a decrease in Young's modulus, significantly [24]. This was noted when the CTBN modifier was employed in an epoxy resin by another study [25]. In the present case, the modification by 25wt% of CTBN permits a change of 56% of Young's modulus. The various tensile properties for different CTBN concentrations of the rubber are formulated in Table 2. The decrease in tensile strength with increasing rubber content can be related to stiffness of the modified network. The addition of rubber decreases the stiffness of the epoxy network probably due to a lowering in cross-linking density.

Typical fractured surfaces of neat and that of 25wt% rubber-modified epoxies at different magnifications are shown in Fig.6. In Figs. 6 (a,b) the crack initiation zone is located at the bottom of the images and it is distinguished by the relatively smooth area. Typically, the neat epoxy matrix shows smooth as well as rivery fractured surfaces with ripples. The ripples occur due to the brittle fracture of the epoxy. On the other hand, the morphology of the rubber modified epoxies are shown in Fig.6 (c,d). In Fig.6(c) the crack initiation zone is probably at the right side of the image since the rest of the image shows significantly higher roughness and distinctive hackle zones. The cavitations illustrated in Fig. 6(d) developed from the rapid crack propagation and finally rupture of the tensile specimens and they are due to the extracted rubber particles after fracture. Additionally, as revealed from the cavitations, the particles were uniformly distributed throughout the epoxy matrix.

4.2. Modal test results

According to the time history results of the vibration tests, the acceleration at the free end of the cantilever beam has been monitored for each sample (Fig.7). Obviously the attenuation rate of vibration deflection is faster when the CTBN content is higher. As shown in Fig.7, the free vibration of the neat epoxy, the amplitude of vibration is attenuated, reaching zero after a large number of cycles. However, it takes only a few cycles for the amplitude to approach zero when free vibration occurs for the 25wt% CTBN rubber sample. Material damping capacity can also be inferred from the comparison between different vibration attenuation rates. The decay time is shown in Table 3. Based on Table 3 and Fig.7, the attenuation time is faster when the CTBN rubber weight fraction is higher.

4.3. Identified transfer functions of the epoxy/rubber specimens

The analytical functions identified the resonance in all three important flexural modes. These mathematically synthesized transfer functions contain all the important resonance information while interpolation among measured data is considered satisfactory. Fig.8 shows the comparison between the identified and measured complex TFs of the specimens.

The identified resonant frequencies of the specimens with different inclusions are shown in Table 4. It is obvious that the frequencies of the first mode increase with respect to the CTBN rubber content. This was expected since the rubber addition decreases the stiffness of the epoxy network due to the lower stiffness of the rubber itself and probably the reduction in cross-linking density.

4.4. Determination of elastic modulus, loss modulus and loss factor with TF method

The first mode of vibration was used in order to calculate the (E') and (E'') moduli. The compliance of each beam specimen was calculated from the experimental and identified by the genetic algorithm transfer functions, while the elastic modulus was determined by Eq.2. Fig.9 shows a good agreement between the elastic moduli determined by tensile tests and the proposed analytical-experimental TF method, considering the absolute differences (Table 5). However, for the case of the experimental TFs, the elastic modulus does not show good approximation with the tensile test results. Thus, the analytical-experimental identification method appears to be essential for the determination of the elastic modulus of the specimens.

The loss modulus is proportional to the (E') and (n) values and it is related to the energy dissipation mechanisms in materials. The loss modulus is a combination of energy dissipation mechanisms from the matrix material, the inclusions and the interface between them. So, in this case, the energy dissipation due to interfacial adhesion can be of major importance.

Table 6 shows the values of the loss factor (n) and the loss modulus (E'') for the tested specimens. The addition of CTBN rubber particles in the epoxy matrix has improved the damping behavior. This improvement induced by the CTBN rubber particles could be attributed to their good dispersion within the epoxy as well as the reduced cross-linking density of epoxy itself. It has been also shown in another study [11] that the damping properties of an epoxy resin can be modified by CTBN rubber particles. The results in the current work verifies the fact that when the epoxy is loaded with 25wt% CTBN particles, the highest loss factor value among the other concentrations can be attained with an improvement of 128% compared with the neat epoxy resin (Table 6).

5. CONCLUSIONS

The dynamic mechanical properties of epoxy modified with different Carboxyl-Terminated Butadiene-Acrylonitrile rubber were investigated with an analytical-experimental modal testing method. The epoxy/CTBN rubber composites were at first tested under uniaxial tension. The samples with high CTBN concentrations revealed a characteristic plastic behavior, although the addition of the CTBN decreased the strength and the Young's Modulus. The strength decrease was significant with noticeable improvement in the strain to failure, revealing a characteristic toughening effect. The decrease in tensile strength with rubber content can be related to the stiffness of the modified network, while the rubber

addition decreases the stiffness of the network epoxy probably due to lowering in cross-linking density. Time history results have shown that the attenuation rate of vibration deflection is faster when the CTBN content is higher, although the peak amplitude reaches higher values. The analytical-experimental transfer function for each composite material has been identified through an optimization algorithm and fundamental modal parameters, as resonant frequency and damping ratio were determined. Given the fact that modal parameters were defined, the elastic modulus of the composite material was deduced. Compared with a static tensile testing method, the proposed method is inexpensive, convenient and accurate. Furthermore, the proposed modal testing method is non-destructive. A numerical example shows that the proposed algorithm is efficient and robust for identifying the modal parameters of 10-DOF linear system. The proposed modal testing results indicate that the addition of CTBN particles significantly improved the damping capacity of the epoxy-based composites. However, it was observed that the stiffness of the epoxy based system was dramatically reduced.

REFERENCES

1. Ewins DJ. Modal testing: Theory and practice, Research Studies Press, John Wiley and Sons, Lechtworth, New York etc., 1984.
2. Adams R. Mechanisms of damping in composite materials. Journal de Physique Colloques 1983; 44 (C9):C9-29-C9-37.
3. Biggerstaff JM, JB Kosmatka. Damping Performance of Cocured Graphite/Epoxy Composite Laminates with Embedded Damping Materials. J Compos Mater 1999; 33: 1457–1469.
4. Kosmatka JB, Liguore SL. Review of Methods for Analyzing Constrained Layer Damping Structures. J Aerosp Eng 1993;6: 268–283.
5. Baz A, Ro J. The Concept and Performance of Active Constrained Layer Damping Treatments. J Sound Vib 1994; 28: 18–21.
6. Liao WH, Wang KW. On The Analysis of Viscoelastic Materials for Active Constrained Layer Damping Treatments. J Sound Vib, 1997; 207: 319–334.
7. Liu Y, Wang KW. A Non-Dimensional Parametric Study of Enhanced Active Constrained Layer Damping Treatments, J Sound Vib, 1999; 223: 611–644.

8. Buldum A, Lu JP. Atomic Scale Sliding and Rolling of Carbon Nanotubes. Phys Rev Lett 1999; 83: 5050–5053.

9. Mansour G, Tzetzis G, Bouzakis KD. A nanomechanical approach on the measurement of the elastic properties of epoxy reinforced carbon nanotube nanocomposites. Tribology In Industry 2013; 35 (3): 190-199.

10. Tzetzis D, Mansour G, Tsiafis I, Pavlidou E. Nanoindentation measurements of fumed silica epoxy reinforced nanocomposites. Journal of Reinforced Plastics and Composites 2013; 32(3): 160–173.

11. Mansour G, Tzetzis D. Nanomechanical characterization of hybrid multiwall carbon nanotube and fumed silica epoxy nanocomposites. Polymer-Plastics Technology and Engineering 2013; 52:1054–1062.

12. Tsai JL, Chang NR. Investigating damping properties of nanocomposites and sandwich structures with nanocomposites. Journal of Composite Materials 2011; 0(0):1-7.

13. Zhao XY, Xiang P, Tian M, Fong H, Jin R And Zhang Lq. Nitrile Butadiene Rubber/Hindered Phenol Nanocomposites with Improved Strength and High Damping Performance. Polymer 2007; 48: 6056–6063, 2007.

14. Sprenger S. Epoxy resins modified with elastomers and surface-modified silica nanoparticles. Polymer 2013; 54:4790–4797.

15. Tzetzis D, Hogg PJ. Bondline toughening of vacuum infused composite repairs, Composites Part A 2006; 37:1239–1251.

16. Tzetzis D, Hogg PJ. The influence of surface morphology on the interfacial adhesion and fracture behavior of vacuum infused carbon fiber reinforced polymeric repairs. Polymer Composites 2008; 29 (1): 92-108.

17. Tzetzis D, Hogg PJ. Infield composites repair techniques for combat aircraft: Research and development perspective. Materials Technology 2007; 22 (1): 2-9.

18. Tzetzis D, Hogg PJ, Jogia M. Double cantilever beam mode-I testing for vacuum infused repairs of GFRP. Journal of Adhesion Science and Technology 2003;17 (3): 309-328.

19. Kennedy CC, Pancu CDP. Use of vectors in vibration measurement and analysis, J. Aeronautical Sciences 1947;14(11):603-625.

20. Brown DL, Allemang RJ, Zimmerman R, Mergeay M. Parameter estimation techniques for modal analysis, SAE Paper No. 790221, 1979.

21. Bruel, Kjaer. Mechanical vibration and shock measurements, pp. 97–112 Denmark, 1984.

22. Coley D. An introduction to genetic algorithms for scientists and engineers, World Scientific Press, 1999.

23. Xiao K. and Ye L. Rate-effect on fracture behavior of core-shell-rubber (CSR)-modified epoxies. Polym Eng Sci 2000; 40: 70–81.

24. Tang, Wang X, Wan YJ, Wu LB, Jiang JX, Lai GQ. Mechanical properties and fracture behaviors of epoxy composites with multi-scale rubber particles. Materials Chemistry and Physics 2013;141: 333-342.

25. Thomas R, Abraham J, Thomas PS, Thomas S. Influence of carboxyl-terminated (butadiene-co-acrylonitrile) loading on the mechanical and thermal properties of cured epoxy blends. J Poly Sci Part B PolymPhys 2004; 42:2531.

ACKNOWLEDGEMENTS

This research was supported by the IKY (Greek State Scholarships Foundation) Fellowships of Excellence Postgraduate Studies program - Siemens. The authors would like to thank Dr. S. Sprenger and Evonik Hanse GmbH for providing the Albipox 1000.

Figure Captions:

Figure 1: Experimental setup of vibration tests.

Figure 2: Complex transfer function of a single degree of freedom system.

Figure 3: Flowchart for the identification process of the genetic algorithm.

Figure 4: Identification of transfer functions of 10-DOF mass-spring-dashpot model and comparison of modal parameters.

Figure 5: Typical stress–strain curves of specimens loaded in static uniaxial tension showing the effect of the CTBN rubber reinforcement.

Figure 6: SEM micrographs of: (a) neat epoxy, (b) neat epoxy at higher magnification, (c) 25wt% rubber modified epoxy, (d) 25wt% rubber modified epoxy at higher magnification showing the rubber particle cavitations.

Figure 7: Typical acceleration measurements of the specimens for different content of CTBN rubber.

Figure 8: Identified complex transfer functions for (a) neat epoxy and (b) CTBN 25wt%.

Figure 9: Comparison of the elastic moduli between TF method and tensile tests of the epoxy/CTBN rubber specimens.

Table 1: Dynamic properties of the 10-degree-freedom mass-spring-dashpot model

Dynamic Property		Mode number									
		1	2	3	4	5	6	7	8	9	10
M	[kg]	156	139	122	105	88	77	54	37	20	3
K	[N/m] x10^6	253	223	193	163	133	103	73.3	43.3	13.3	13.3
C	[Ns/m]x10^3	11.3	10	8.75	7.46	5.42	4.08	3.55	2.28	0.93	0.36

Table 2: Mechanical properties at room temperature of neat epoxy and with different loading of CTBN rubber postcured at 50°C for 16hr.

Engineering Constant		Neat epoxy	CTBN (wt%)			
			10	15	20	25
Young's modulus	[MPa]	3815 ± 120	3245 ± 147	2630 ± 112	2037 ± 144	1686 ± 151
Ultimate tensile strength	[MPa]	67 ± 2	52 ± 1	41 ± 4	20 ± 2	17 ± 4
Strain	[%]	1.83 ± 0.13	2.22 ± 0.11	2.58 ± 0.7	2.73 ± 0.6	2.84 ± 0.13

Table 3: Attenuation time of neat epoxy specimens and epoxy mixed with different CTBN at different loadings.

Property	Neat Epoxy	CTBN 10wt%	CTBN 15wt%	CTBN 20wt%	CTBN 25wt%
Attenuation time [s]	0.85	0.80	0.70	0.46	0.20

Table 4: Resonant frequencies of the important flexural modes of the specimens.

Specimen	First frequency [Hz]	Second frequency [Hz]	Third frequency [Hz]
Neat epoxy resin	83.50	445.00	1232.50
CTBN 10wt%	72.50	402.50	924.50
CTBN 15wt%	69.50	382.50	853.50
CTBN 20wt%	55.50	332.50	799.50
CTBN 25wt%	49.50	258.50	766.50

Table 5: Elastic moduli of the epoxy/CTBN rubber specimens determined with experimental and GA identified TFs compared to tensile tests.

Specimen	Elastic Modulus [MPa]				
	Tensile tests	Experimental TF method	Absolute difference	Identified TF method	Absolute difference
Neat epoxy resin	3815	4809	26%	4017	5%
CTBN 10wt%	3245	4165	28%	3061	6%
CTBN 15wt%	2630	3327	26%	2828	8%
CTBN 20wt%	2037	2593	27%	1814	11%
CTBN 25wt%	1686	2112	25%	1451	14%

Table 6: Loss moduli and loss factors of the specimens.

Specimen	E'' [MPa]	Loss factor n	Improvement of the loss factor (%)
Neat epoxy resin	147.82	0.0368	-
CTBN 10wt%	163.46	0.0534	45
CTBN 15wt%	173.67	0.0614	67
CTBN 20wt%	123.69	0.0682	85
CTBN 25wt%	121.57	0.0838	128

Experimental setup

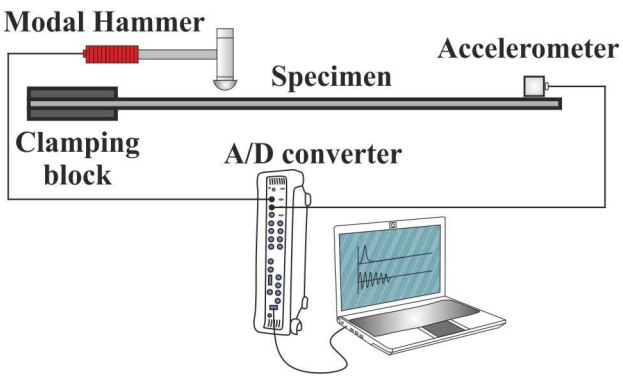

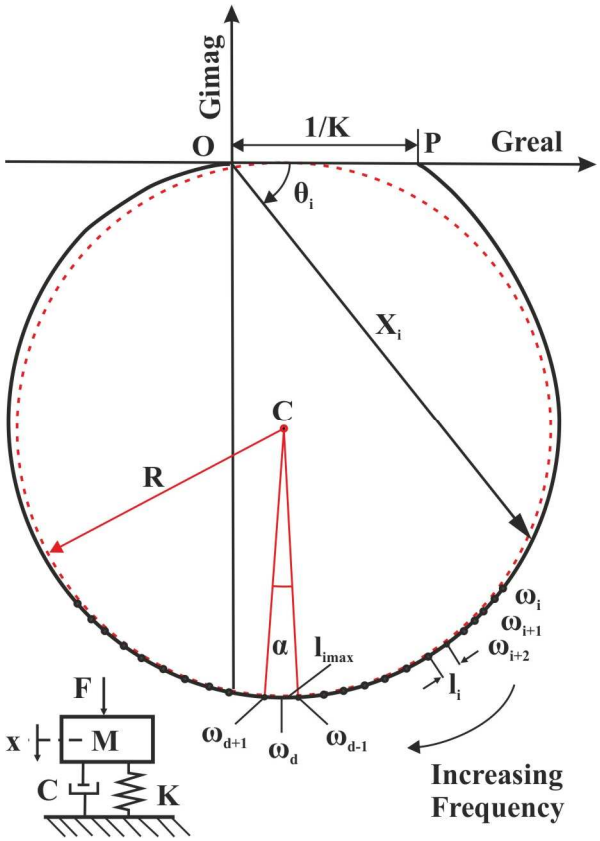

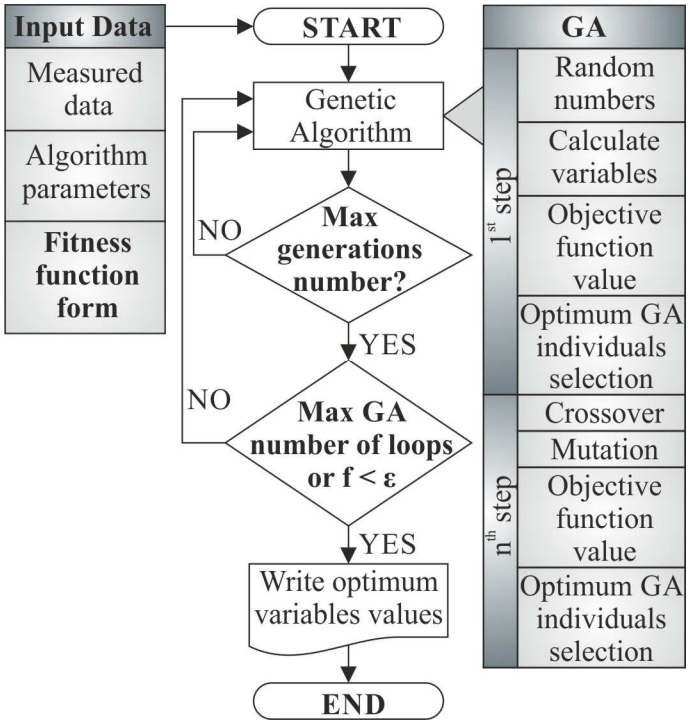

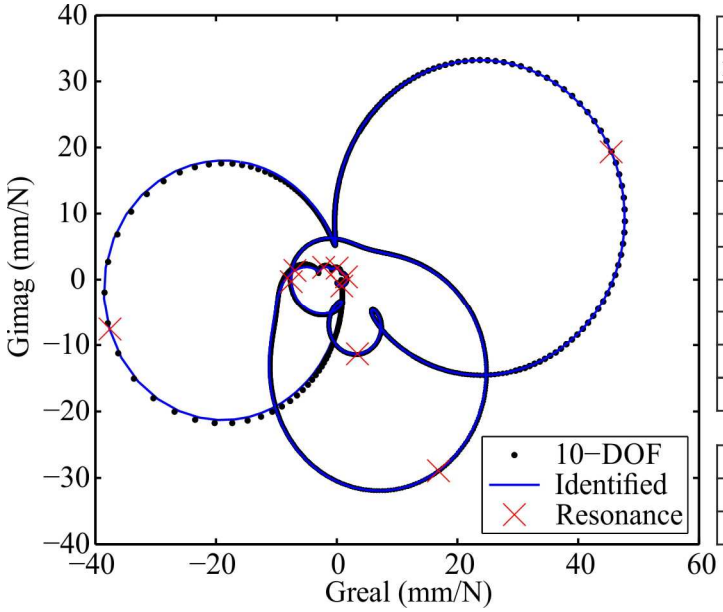

	10-DOF		Identified	
mode	ω_d (Hz)	n	ω_d (Hz)	n
1	279	0.0354	279	0.0356
2	571	0.0556	571	0.0558
3	823	0.0654	824	0.0662
4	1120	0.0632	1120	0.0646
5	1410	0.0938	1410	0.0914
6	1700	0.0778	1690	0.0779
7	1920	0.0938	1910	0.0930
8	2140	0.0912	2130	0.0848
9	2250	0.0646	2237	0.0682
10	2340	0.0800	-	-
•	•	•	•	•
8	2140	0.0912	2140	0.0901
9	2250	0.0646	2240	0.0656
10	2340	0.0800	2370	0.0888

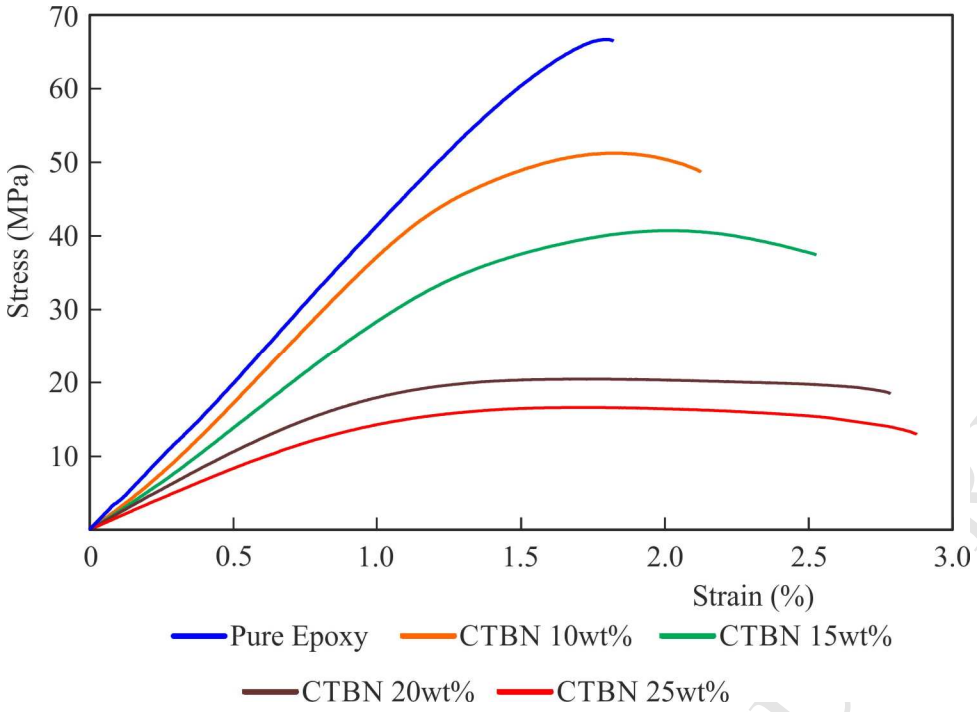

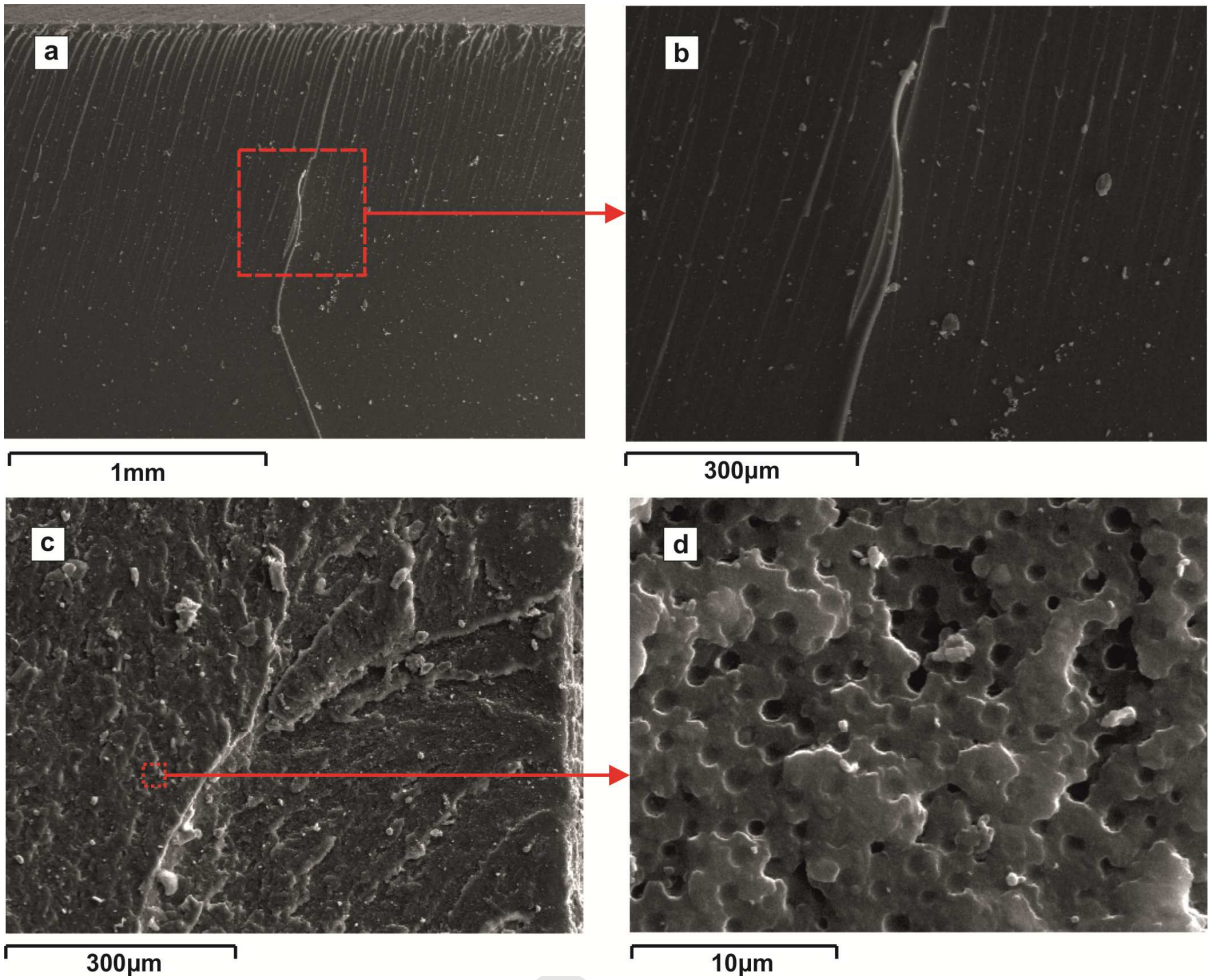

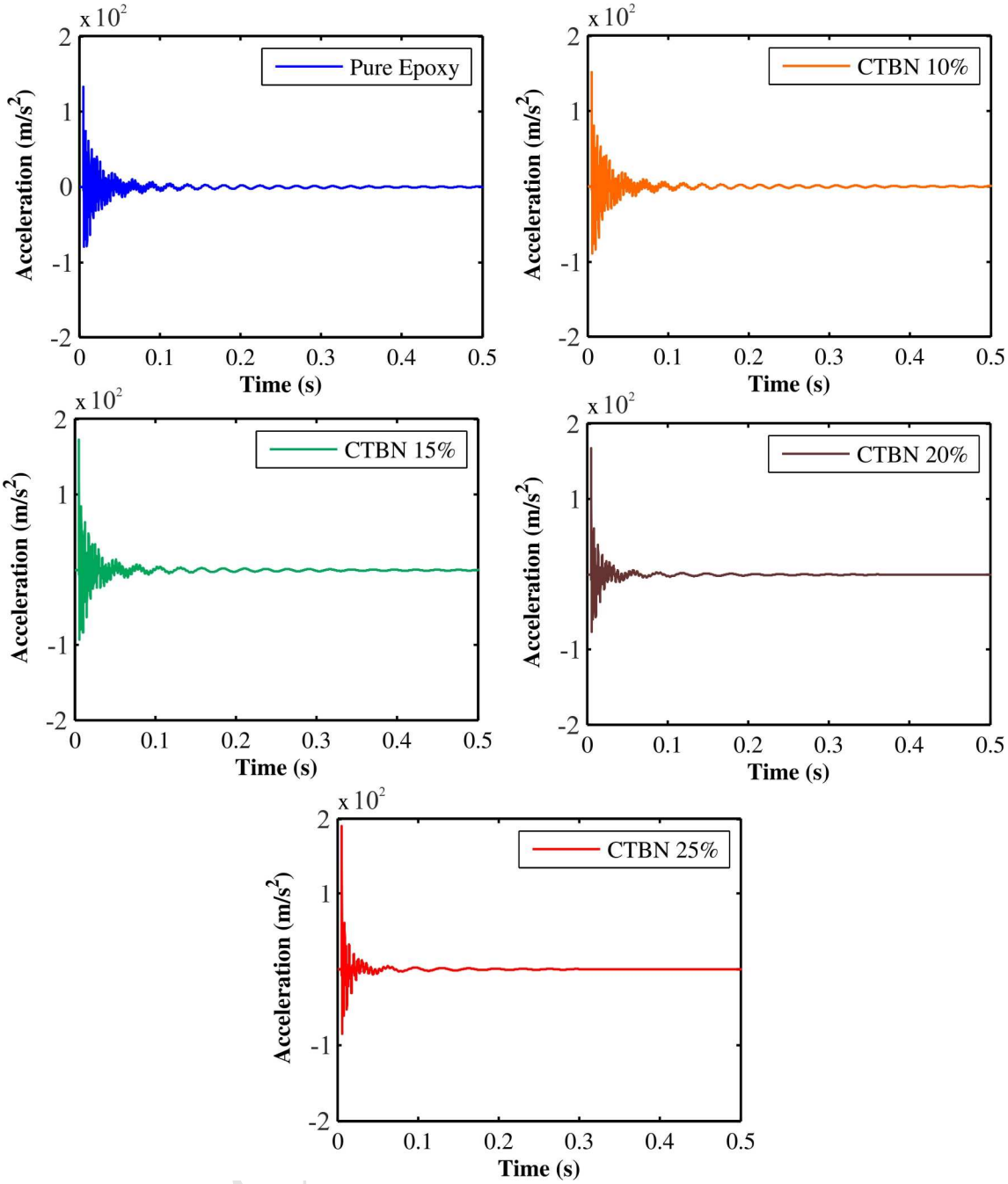
x 10^2
Pure Epoxy
Acceleration (m/s^2)
Time (s)
CTBN 10%
CTBN 15%
CTBN 20%
CTBN 25%